Organic & Biomolecular Chemistry

Cite this: *Org. Biomol. Chem.*, 2011, **9**, 6410

www.rsc.org/obc

**PAPER**

# Synthesis, structures, redox and photophysical properties of benzodifuran-functionalised pyrene and anthracene fluorophores†

**Stephan Keller,[a] Chenyi Yi,[a] Chen Li,[a] Shi-Xia Liu,*[a] Carmen Blum,[a] Gabriela Frei,[a] Olha Sereda,[b] Antonia Neels,[b] Thomas Wandlowski[a] and Silvio Decurtins[a]**

***Received 18th May 2011, Accepted 17th June 2011***
**DOI: 10.1039/c1ob05778b**

Benzodifuran-functionalised pyrene and anthracene fluorophores **1** and **2** were obtained in reasonable yields. Their single crystal structures, electrochemical, optical absorption, and fluorescence characteristics have been described. They show strong luminescence with high quantum yields of 0.53 for **1** and 0.48 for **2**.

## Introduction

This paper puts forward a study of largely extended π-conjugated molecules, resulting from combining through ethynyl spacers a recently developed redox-active chromophore, namely a benzodifuran (BDF) derivative,[1] with two pending pyrene or anthracene fluorophores, respectively. The motivation is triggered by the fascinating features of these individual components.

Derivatives of benzofuran and benzodifuran show a wide range of biological activities that put them within the focus of bioorganic and medical research.[2] Benzodifuran derivatives have also proven to be excellent compounds in the field of molecular electronics, especially for hole-transporting materials.[3]

Pyrene and anthracene, as strong π–π* emitters, have been previously employed as fluorescent probes in many applications. For example, anthracene chromophores can be used to signal environmental effects that help to delineate inter/intramolecular interactions.[4] Pyrene is one of the most frequently used compounds for oligonucleotide labelling.[5] Pyrene-based fluorescent probes are also used to monitor conformational changes by virtue of their excimer fluorescence (for example in the case of the natural iron chelator myo-inositol 1,2,3-triphosphate).[6] Analogously, the face-to-face orientation excimer emission of pyrene units is applied in chemosensor systems,[7] or used for reporting lipid-protein interactions in membranes.[8] However, they have serious drawbacks such as a relatively short absorption wavelength, substantial fluorescence quenching in the presence of oxygen and low fluorescence quantum yields. It has been found that the introduction of alkynyl groups into pyrene/anthracene leads to effective extension of the π–conjugation and a large increase of fluorescence intensities even under aerated conditions.[9] Taking these features into account, we herein report the synthesis, photophysical properties and spectroelectrochemistry of two new acetylene-linked benzodifuran-functionalised pyrene and anthracene fluorophores.

The ability of the functionalised benzodifuran core to undergo Suzuki, Heck and Sonogashira coupling reactions has been demonstrated in the case of pyridyl substituents.[1] Thereby, an extended π-conjugated molecular platform is created, which allows for photoinduced intramolecular charge-transfer processes to occur. Therefore, as a part of a continuing research effort in the development of new materials for molecular electronics, we herein describe the synthesis of compounds **1** and **2** (Scheme 1), and their characterisation in solution and in the solid state.

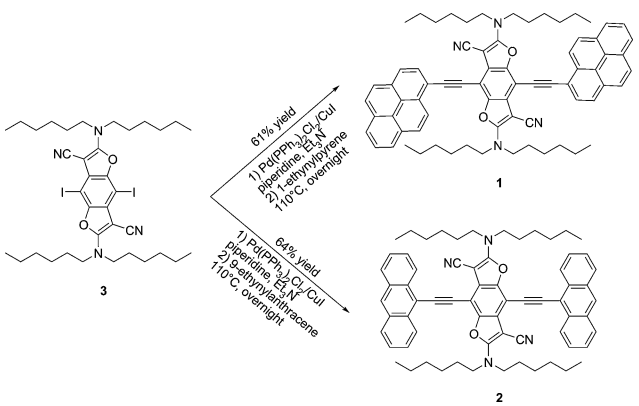


**Scheme 1** Synthesis of compounds **1–2**.

## Results and discussion

### Synthesis

Our interest in malonitrile chemistry,[10] recently led us to an efficient synthetic approach to a fully functionalized benzodifuran

[a]*Departement für Chemie und Biochemie, Universität Bern, Freiestrasse 3, CH-3012, Bern, Switzerland. E-mail: liu@iac.unibe.ch; Fax: +41 31 6313995; Tel: +41 31 6314296*

[b]*XRD Application LAB, CSEM Centre Suisse d'Electronique et de Microtechnique SA, Jaquet-Droz 1, Case postale, CH-2002, Neuchâtel, Switzerland*

† Electronic supplementary information (ESI) available: Additional information on the computational studies of compounds **1** and **2**. See DOI: 10.1039/c1ob05778b

molecule **3** (Scheme 1), which can readily undergo Suzuki, Heck, and Sonogashira coupling reactions to afford extended π-conjugated BDF derivatives with pyridine termini through different spacers.[1] As illustrated in Scheme 1, pyrene and anthracene fluorophores can be incorporated into the BDF core *via* a Pd-catalyzed Sonogashira coupling reaction of **3** with the corresponding 1-ethynylpyrene and 9-ethynylanthracene, leading to the formation of compounds **1** and **2** in reasonable yields. 1-Ethynylpyrene and 9-ethynylanthracene were accomplished according to modified literature procedures, starting from iodo- or bromo-substituted pyrene and anthracene through a Sonogashira coupling and subsequent desilylation. In both cases, yields are comparable to or even better than those reported.[11,12]

## X-Ray studies

Slow evaporation of a saturated dichloromethane solution of **1** produced solvate-free orange needle-shaped crystals suitable for X-ray diffraction. The compound crystallizes in the monoclinic space group $P2_1/c$ (No. 14) with one molecule per asymmetric unit. The ORTEP diagram is illustrated in Fig. 1. The BDF core is fairly planar; the rms deviation from the least-squares plane through the heterocyclic BDF skeleton is 0.44 Å. The dihedral angles formed between the pyrene rings and the BDF unit are 19.3(2)° and 17.6(2)°, respectively. Clearly, the orientation of the pyrene units is such as to avoid close contacts with the nitrile groups. There are no exceptional geometrical features, and all bond lengths and angles are within the expected range; they compare with the reported structures of BDF derivatives.[1] In the crystal lattice, the molecules show stacking along the crystallographic *b*-axis. A π–π stacking is observed between alternating aromatic BDF units and the pyrene parts. The shortest intermolecular distances related to these π–π interactions are found with 3.30 Å for C17 . . . C50$^{i}$ (symmetry operation i: –x, –y+1, –z) and 3.52 Å for C19 . . . C69$^{ii}$ (symmetry operation ii: –x+1, –y+1, –z), respectively.

Slow evaporation of a saturated dichloromethane solution of **2** produced a mixture of solvate-free orange rod-shaped (**2a**) and block-shaped (**2b**) crystals suitable for X-ray diffraction. Compound **2** crystallizes for both morphologies in the monoclinic space group $P2_1/c$ (No. 14) with one half molecule per asymmetric unit; the corresponding ORTEP diagrams are illustrated in Fig. 2. In the solid state, a crystallographic inversion centre is located at the central $C_6$ ring for **2a** and **2b**. The BDF cores are nearly planar; the rms deviations from the least-squares planes through the heterocyclic BDF skeletons are 0.01 Å and 0.03 Å for **2a** and **2b**, respectively. The dihedral angles formed between the anthracene units and the BDF units are very different in the two structures and have been calculated with 1.8(1)° (**2a**) and 28.45(1)° (**2b**). There are no exceptional geometrical features, and all bond lengths and angles are within the expected range. They compare with the reported structures of BDF derivatives.[1]

In the crystal lattice of **2a**, the molecules show a ladder like stacking of alternating BDF and anthracene moieties in two directions which results in an interwoven pattern. The smallest carbon-carbon distance involved in the intermolecular stacking network was found with 3.27 Å for C18 . . . C28$^{i}$ (symmetry

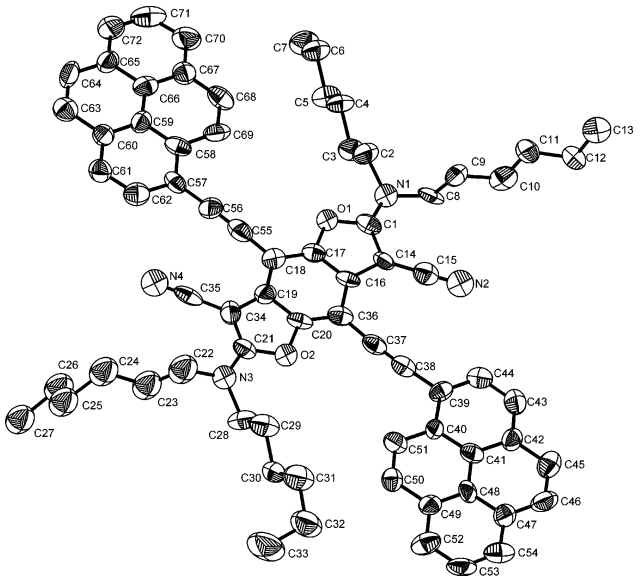


**Fig. 1** Solid state structure of **1**. Thermal ellipsoids are set at the 50% probability level and hydrogen atoms are omitted for clarity.

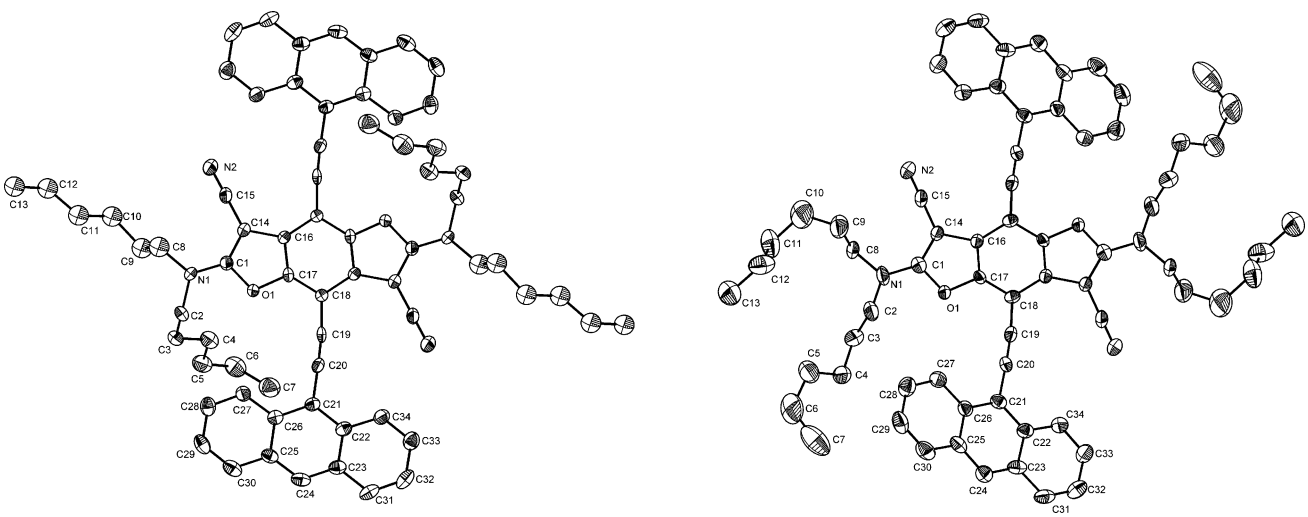


**Fig. 2** Solid state structures of **2a** (left) and **2b** (right). Thermal ellipsoids are set at the 50% probability level and hydrogen atoms are omitted for clarity.

operation i: –x+1, –y+2, –z). No special features have been identified for **2b**.

### Electrochemistry

The electrochemical properties of **1–3** were investigated by cyclic voltammetry in $CH_2Cl_2$ (Fig. 3). All compounds undergo one reversible oxidation process with $E_{1/2}^1$ = 0.85 V for **1**, 0.86 V for **2** and 0.97 V for **3**, values that are characteristic for the formation of the respective BDF radical cations.[1,13] The first oxidation potentials of **1** and **2** are quite similar and negatively shifted when compared to **3**. This finding can be attributed to the stabilisation effect of the extended π-conjugation, which offers the possibility of the free spin to be delocalised over the entire conjugated π-system. The formation of the corresponding BDF dication is represented clearly in a second reversible oxidation process for **3** with $E_{1/2}^2$ = 1.23 V. In contrast, this process is not electrochemically reversible in the cases of **1** and **2**. Extending the potential range to 1.4 V reveals for **1** a distorted anodic peak with $E_{pa}$ = 1.18 V, and four successive cathodic peaks at $E_{pc}^1$ = 0.86 V, $E_{pc}^2$ = 0.94 V, $E_{pc}^3$ = 1.05 V and $E_{pc}^4$ = 1.16 V. Compound **2** shows an anodic peak at $E_{pa}$ = 1.26 V and a corresponding cathodic peak at $E_{pc}$ = 1.06 V. To gain insight into the potential evolution of the redox behaviour of **1**, a "window-opening" CV experiment was performed by extending the positive potential limit from 1.0 V to 1.5 V (Fig. 4). All cathodic peaks appear only upon the oxidation of the BDF radical cation to dication species. Furthermore, it is found that the charge consumption between the anodic and the cathodic scans is not idential. These observations are indicative of an electron-transfer reaction, most probably coupled with a complex sequence of chemical follow-up processes.

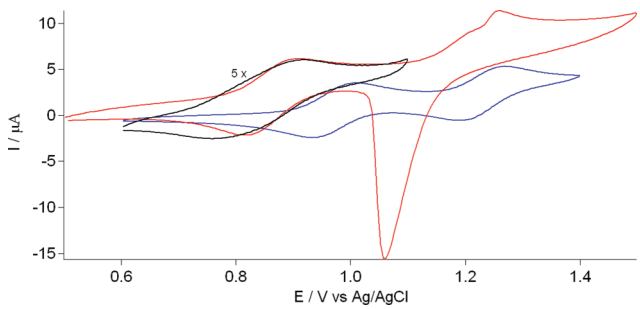


**Fig. 3** Cyclic voltammograms of **1** ($1 \times 10^{-4}$ M, black), **2** ($5 \times 10^{-4}$ M, red) and **3** ($2 \times 10^{-4}$ M, blue) in $CH_2Cl_2$ (0.1 M $TBAPF_6$ (TBA = tetrabutylammonium)); platinum disk working electrode; scan rate 100 $mVs^{-1}$).

### Electronic properties

In order to evaluate the frontier molecular orbitals (MOs) for **1** and **2**, *ab initio* quantum chemical calculations were performed, employing density functional theory with the B3LYP functional and the valence triple-ζ plus polarization basis set. The calculations were carried out with the TURBOMOLE V6.0 program package.[14] The ground-state optimized structures (see ESI†) of both compounds (with $NH_2$ instead of N(hexyl)$_2$ groups) were constrained to $C_{2h}$ symmetry. Some frontier molecular orbitals are given in Fig. 5 and 6. The MO schemes appear analogous for both compounds. The electron densities of the highest occupied MO (HOMO) and the lowest unoccupied MO (LUMO) are

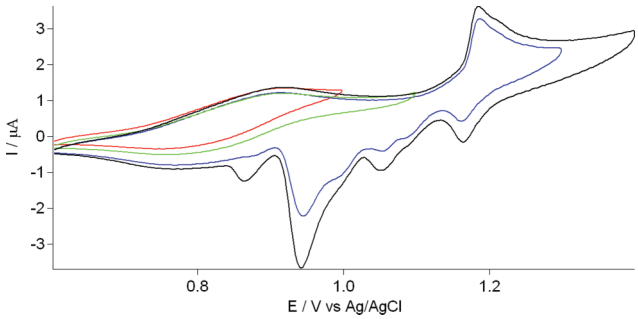


**Fig. 4** "Window-opening" cyclic voltammograms of **1** ($1 \times 10^{-4}$ M) in $CH_2Cl_2$ (0.1 M $TBAPF_6$ (TBA = tetrabutylammonium)); platinum disk working electrode; scan rate 100 $mVs^{-1}$, with different positive potential limits.

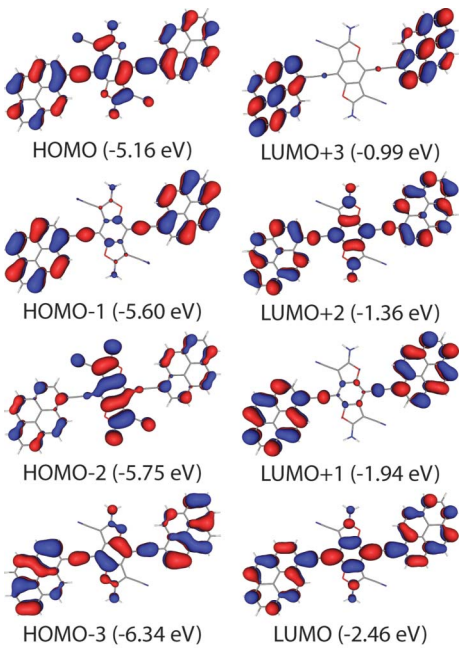


**Fig. 5** Molecular orbitals of **1**.

extended over the whole molecule; in fact and as expected, they are formed by symmetry-adapted linear combinations of the respective HOMOs or LUMOs of the pending groups with the HOMO or LUMO of BDF. The calculated HOMO–LUMO gap results in a value for **1** of 2.7 eV (21800 $cm^{-1}$) and for **2** of 2.5 eV (20200 $cm^{-1}$); both energies are comparable with those of the onsets of the first absorption band of the optical spectra.

The electronic spectra of the orange colored compounds **1** and **2**, recorded in dichloromethane solution, show intense optical absorptions over the UV-vis spectral part with absorption onset energies at about 18400 $cm^{-1}$ (543 nm) and 18100 $cm^{-1}$ (552 nm), respectively (Fig. 7 and 8). As expected, both compounds exhibit a quite similar absorption pattern. Based on the detailed spectral analysis of the related BDF derivative with pending 4-ethynylpyridine groups[1] and on the comparison with the electronic absorption spectra of the fragmental chromophoric moieties of **1** and **2**, the main characteristics of the electronic transitions can be explained. Firstly, at low wavelength a strong and broad absorption band appears around 20400 $cm^{-1}$ (490 nm) for **1**

 

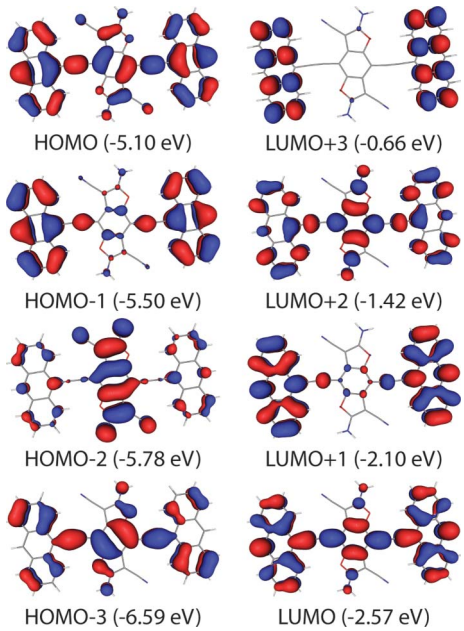


**Fig. 6** Molecular orbitals of **2**.

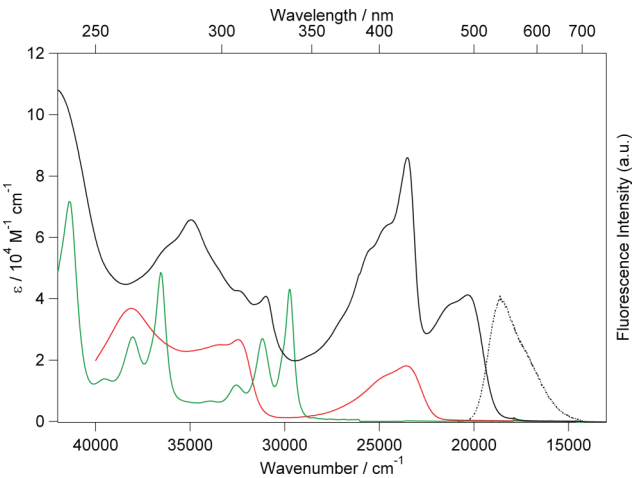


**Fig. 7** Electronic absorption (black solid line) and fluorescence emission (dashed line) spectra of **1** in deaerated dichloromethane solution at room temperature together with absorption spectra of the reference compounds 1-ethynylpyrene (green line) and 2,6-bis(dihexylamino)-4,8-diethynylbenzo[1,2-*b*:4,5-*b*′]difuran-3,7-dicarbonitrile (red line).

and 20900 $cm^{-1}$ (480 nm) for **2**, which can only be observed in such π–extended chromophores. Based on the vertical TD-DFT calculation for the $S_0 \rightarrow S_1$ electronic excitation observed at 20800 $cm^{-1}$ (481 nm) in case of the BDF(–≡–pyridine)$_2$ analogue,[1] one may predict that this lowest-energy band of **1** and **2** substantially corresponds to an excitation described by a one-electron HOMO→LUMO promotion. Comparing it with the frontier molecular orbitals one recognizes clearly that the involved π–π* transition represents an electronic redistribution over the whole molecule and there is no localisation on either the BDF core or on the pending groups. Secondly, the intense absorptions between 22000 $cm^{-1}$ (455 nm) and 25000 $cm^{-1}$ (400 nm) originate to a larger extent from BDF-based π–π* transitions and thirdly, at higher energies the π–π* transitions of the pending groups

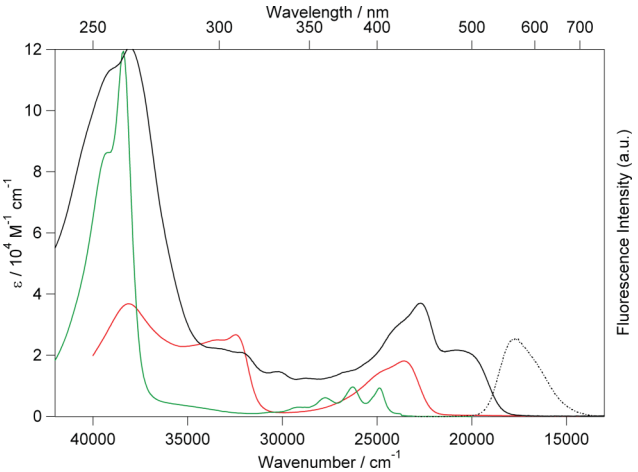


**Fig. 8** Electronic absorption (black solid line) and fluorescence emission (dashed line) spectra of **2** in deaerated dichloromethane solution at room temperature together with absorption spectra of the reference compounds 9-ethynylanthracene (green line) and 2,6-bis(dihexylamino)-4,8-diethynylbenzo[1,2-*b*:4,5-*b*′]difuran-3,7-dicarbonitrile (red line).

are increasingly contributing to the overall absorption pattern.[1] Furthermore, the chromophoric molecules **1** and **2** show strong fluorescence emission in dichloromethane solution (Fig. 7 and 8) at 18400 $cm^{-1}$ (543 nm) and 17700 $cm^{-1}$ (565 nm) with Stokes shifts of $\nu_{ST}$ = 2000 $cm^{-1}$ and 2700 $cm^{-1}$, respectively. The corresponding luminescence quantum yields $\Phi_F$ are quite high with values of 0.53 and 0.48, respectively.

### Spin delocalisation as seen through spectroelectrochemical studies

Systematic changes in the optical spectra upon oxidation of the neutral species **1–3** were examined by spectroelectrochemistry, as shown in Fig. 9.

Fig. 9a shows the variation of the absorbance spectra of **1** at seven consecutive applied potentials that lead to the monocationic species **1**$^{\bullet+}$. As the potential shifts positively, it is observed that the lowest-energy 20400 $cm^{-1}$ (490 nm) peak gradually decreases leading to an isosbestic point at 21500 $cm^{-1}$ (465 nm) since a close lying new absorption band appears. The higher energy intense absorptions which bear strong BDF core character decrease significantly, indicating the participation of the BDF central core in the process. This result is in qualitative agreement with the aforementioned interpretation of the electrochemical data. On the other hand, in the wavelength range 18000–10000 $cm^{-1}$ (555–1000 nm), four highly structured absorption bands ($\lambda_{max}$ = 610, 670, 760, 855 nm) appear. Importantly, all of the spectra shown in Fig. 9 have this character; these bands are thus characteristic of the BDF π-radical cation. Additionally, **1** shows one intense NIR absorption band ($\lambda_{max}$ = 1130 nm, 8850 $cm^{-1}$) upon the first oxidation, which can probably be ascribed to the formation of the dimeric radical cation species of the BDF cores (π-dimers) arising from strong intermolecular π–π interactions.

Fig. 9b exhibits the absorption spectra of **2** taken at the indicated potentials. Similar to **1**, four well-defined absorption bands ($\lambda_{max}$ = 620, 680, 775, 880 nm) and one broad band ($\lambda_{max}$ = 1250 nm, 8000 $cm^{-1}$) appear upon the first oxidation. Significantly for **2**, a new strong absorption band at 19200 $cm^{-1}$ (520 nm) accompanied by an isosbestic point at 19800 $cm^{-1}$ (505 nm) is observed. The

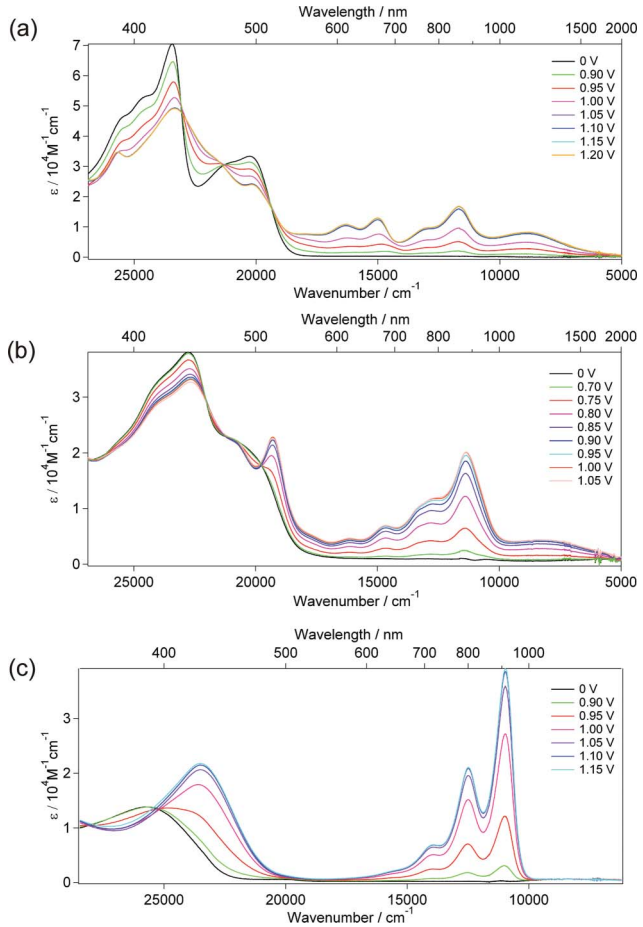


**Fig. 9** UV-visible spectral changes of **1** (a), **2** (b) and the precursor **3** (c) during the first oxidation in $CH_2Cl_2$, 0.1 M $TBAPF_6$.

spectral evolution of the BDF precursor **3** during the first oxidation is shown in Fig. 9c. As the oxidation proceeds, the original lowest-energy absorption band at 25600 $cm^{-1}$ (390 nm) decreases and a new band at 23300 $cm^{-1}$ (430 nm) raises. Importantly, as mentioned above, the new and well structured absorption pattern below 20000 $cm^{-1}$ underpins clearly the signature of the newly formed radical species.

Notably, there is not even a small rising from the baseline below the 10000 $cm^{-1}$ while forming the species $\mathbf{3}^{\bullet+}$, as seen in Fig. 9c. This finding indicates that the spontaneous self-association of $\mathbf{3}^{\bullet+}$ to form a dimer does not take place. In contrast, both $\mathbf{1}^{\bullet+}$ and $\mathbf{2}^{\bullet+}$ show a strong tendency to undergo an intermolecular π-dimerization owing to the stabilisation effect arising from the strong π–π interactions. It can therefore be deduced that the intermolecular π–π interactions are significantly enhanced *via* the fusion of pyrene and anthracene units to the BDF core.

## Conclusions

Benzodifuran-functionalised pyrene and anthracene fluorophores **1** and **2** were obtained in reasonable yields. An experimental and computational study (MO schemes) on their electrochemical, optical absorption, and fluorescence characteristics has been described. The redox-active fluorophores **1** and **2** exhibit various electronic charge-transfer transitions in both neutral and radical cation states leading to intense optical absorbances over a wide spectral range. The electrochemical oxidations of **1** and **2** lead to the appearance of a broad absorption band in the NIR region due to the significantly enhanced intermolecular π–π interactions which originates from the fusion of pyrene and anthracene units to the BDF core. The direct observation of such intermolecular dimerizations in solution at room temperature is still quite challenging as the intermolecular interactions are usually too weak for a dimerization of the radical units to occur. A strong fluorescence emission is also observed at 18400 $cm^{-1}$ (543 nm) and 17700 $cm^{-1}$ (565 nm) for **1** and **2**, respectively, with large Stokes shifts; quantum efficiencies being 0.53 for **1** and 0.48 for **2**.

In search of an electrically triggered luminescence signal from a molecular junction, π-extended BDF derivatives with two terminal pyrene groups are expected to be very promising molecular scaffolds due to their planarity and their strong fluorescence with high quantum yields. Recently, Krupke *et al.* reported the electroluminescence from a single nanotube - molecule - nanotube junction.[15] Therefore, tests of the electroluminescence of the aforementioned π-conjugated systems **1** and **2** trapped in nanogaps, such as between leads of carbon rods, will be of particular interest.

## Experimental section

Air and/or water-sensitive reactions were conducted under $N_2$ in dry, freshly distilled solvents. Unless stated otherwise, all other reagents were purchased from commercial sources and used without additional purification. 2,6-Bis(dihexylamino)-4,8-diiodobenzo[1,2-*b*:4,5-*b*′]difuran-3,7-dicarbonitrile (**3**) was synthesized according to the literature.[1] 1-(Trimethylsilanylethynyl)pyrene, 1-ethynylpyrene, (anthracen-9-ylethynyl)trimethylsilane and 9-ethynylanthracene were accomplished according to modified literature procedures.[11,12] All $^1$H NMR and $^{13}$C NMR spectra were measured at 300 and 75.5 MHz, respectively. Chemical shifts ($\delta$) were calibrated against TMS as an internal standard. UV-vis absorption and emission spectra were recorded on a Perkin-Elmer Lambda 10 spectrometer, a Perkin-Elmer Lambda 900 spectrometer and a Perkin-Elmer Spectrophotometer LS50B. Mass spectra were recorded with an LTQ Orbitrap XL spectrometer for the ESI ionisation mode. Fluorescent quantum yields were referred to diphenylanthracene in EtOH with a quantum yield of 0.9[16] for **1** and rhodamine 6G in EtOH with a quantum yield of 0.95[17] for **2**.

Electrochemical UV/vis/NIR spectra were measured in a commercial spectroelectrochemical cell (BAS, Inc) on a Perkin-Elmer Lambda 900 spectrophotometer at room temperature. The cell is the combination of a thin-layer electrochemical vessel and a quartz cuvette (light path length 1 mm). The sample solutions were dichloromethane (HPLC grade, Acros) containing 0.2 mM BDF derivatives and 0.1 M $TBAPF_6$ (tetrabutylammomium hexafluorophosphate, electrochemical grade, Fluka) as the supporting electrolyte. A gold minigrid was used as working electrode. A platinum wire and a $Ag/AgO_x$ wire served as counter and reference electrodes, respectively. The electrochemical potential was controlled by a lab-built potentialstat.[18] The electrochemical environment was protected from oxygen by purging Ar moderately.

Blank solution was first measured as background. The potential was initially stabilized in the potential region where BDFs

 

maintain their neutral states. The potential applied was adjusted in steps of 0.05 V or 0.10 V towards more positive values, *i.e.* BDF was oxidized to the radical cation. The UV/vis/NIR absorption spectra were recorded *ca.* 2 min after each potential step. The spectra show full reversibility with potential alteration.

### Crystallography

Single crystals of **1** (0.50 × 0.10 × 0.05 mm), **2a** (0.30 × 0.18 × 0.08 mm) and **2b** (0.10 × 0.10 × 0.05 mm) were used for X-ray structure determinations, with diffraction data being collected at low temperature (173 K) on a Stoe Mark II-Image Plate Diffraction System[19] with monochromated graphite Mo-Kα radiation, $\lambda = 0.71073$ Å.

Crystal data. **1** (CCDC 783323): $C_{72}H_{70}N_4O_2$, $M_r$ = 1023.32 gmol$^{-1}$, monoclinic, space group $P2_1/c$, $a$ = 15.8530(13), $b$ = 15.5929(15), $c$ = 25.462(2) Å, $\beta$ = 115.951(6)°, $V$ = 5659.4(8) Å$^3$, $Z$ = 2. 38921 reflection measured, 10102 unique ($R_{int}$ = 0.3199). The measured 2$\theta$ range was 3.07–51.98° corresponding to $d_{max}$–$d_{min}$ = 23.107–0.802 Å. **2a** (CCDC 783324): $C_{68}H_{70}N_4O_2$, $M_r$ = 975.28 gmol$^{-1}$, monoclinic, space group $P2_1/c$, $a$ = 13.7947(9), $b$ = 9.0999(6), $c$ = 22.2042(16) Å, $\beta$ = 105.631(5)°, $V$ = 2684.2(3) Å$^3$, $Z$ = 2. 15649 reflection measured, 4982 unique ($R_{int}$ = 0.0867). The measured 2$\theta$ range was 3.07–51.98° corresponding to $d_{max}$–$d_{min}$ = 23.107–0.802 Å. **2b** (CCDC 783325): $C_{68}H_{70}N_4O_2$, $M_r$ = 975.28 gmol$^{-1}$, monoclinic, space group $P2_1/c$, $a$ = 12.0856(10), $b$ = 17.2822(16), $c$ = 16.4631(16) Å, $\beta$ = 129.164(6)°, $V$ = 2666.1(4) Å$^3$, $Z$ = 2. 13637 reflection measured, 4685 unique ($R_{int}$ = 0.1203). The measured 2$\theta$ range was 3.07–51.98° corresponding to $d_{max}$–$d_{min}$ = 23.107–0.802 Å. The structures were solved by direct methods using the programme SHELXS-97.[20] The refinement and all further calculations were carried out using SHELXL-97.[20] The H-atoms were included in calculated positions and treated as riding atoms. The non-H atoms were refined anisotropically, using weighted full-matrix least-squares on $F^2$.

### Synthesis

**1-(Trimethylsilanylethynyl)pyrene[11].** A mixture of 1-bromopyrene (560 mg, 2 mmol), $Pd(PPh_3)_2Cl_2$ (175 mg, 0.25 mmol), CuI (50 mg, 0.26 mmol) and piperidine (4 mL) in triethylamine (30 mL) was bubbled with $N_2$ for 10 min., and then trimethylsilylacetylene (0.6 mL, 4.1 mmol) was added. The resulting solution was heated at 110 °C overnight in an inert atmosphere. The volatile was evaporated by rotavapor and the residue was subjected to column chromatography on silica gel, eluting with hexane to yield a pale yellow crystalline product (450 mg, 75%). It was characterized by $^1$H NMR giving the same analytical data as reported in the literature.

**1-Ethynylpyrene[11].** A mixture of 1-(trimethylsilyl)ethynylpyrene (420 mg, 1.4 mmol) and tetrabutylammonium fluoride trihydrate (620 mg, 2 mmol) in THF (15 mL) was stirred at room temperature for 1h. The volatile was evaporated by rotavapor and the residue was subjected to column chromatography on silica gel, eluting with hexane to yield a white crystalline product (300 mg, 95%). $^1$H NMR (300 MHz, $CDCl_3$) $\delta$ 8.56 (d, 1H, $J$ = 9 Hz), 8.22–8.03 (m, 8H), 3.62 (s, 1H).

**Compound 1.** A mixture of **3** (200 mg, 0.25 mmol), $Pd(PPh_3)_2Cl_2$ (50 mg, 0.07 mmol), CuI (30 mg, 0.15 mmol) and piperidine (2 mL) in triethylamine (30 mL) was bubbled with $N_2$ for 10 min., and then 1-ethynylpyrene (160 mg, 0.70 mmol) was added. The resulting solution was heated at 110 °C overnight in an inert atmosphere. The volatile was evaporated by rotavapor and the residue was subjected to column chromatography on silica gel, eluting initially with hexane, then with 1 : 1 hexane: $CH_2Cl_2$ to yield an orange solid product (150 mg, 61%). $^1$H NMR (300 MHz, $CDCl_3$) $\delta$ 8.72 (d, 2H, $J$ = 6.0 Hz), 8.52 (d, 2H, $J$ = 7.9 Hz), 8.11 (d, 4H, $J$ = 8.1 Hz), 8.04–7.90 (m, 10H), 3.74 (t, 8H, $J$ = 7.7 Hz), 1.85 (m, 8H), 1.45(m, 8H), 1.29 (m, 16H), 0.81 (t, 12H, $J$ = 6.8 Hz). $^{13}$C NMR (75.4 MHz, $CDCl_3$) $\delta$ 163.2, 145.2, 131.6, 131.4, 131.2, 130.9, 130.0, 128.2, 128.1, 127.2, 126.0, 125.6, 125.5, 125.4, 124.8, 124.3, 123.1, 117.9, 116.8, 99.5, 96.3, 86.1, 62.9, 50.3, 31.7, 28.8, 26.4, 22.6, 14.0; ESI-MS Calc. for $C_{72}H_{70}O_2N_4$ 1022.5499, found 1022.5495.

**(Anthracen-9-ylethynyl)trimethylsilane[12].** A mixture of 9-bromanthracene (1.028 g, 4 mmol), trimethyl-silylacetylene (1.4 mL, 10 mmol), $Pd(PPh_3)_2Cl_2$ (300 mg, 0.43 mmol), CuI (80 mg, 0.4 mmol) and piperidine (2 mL) in triethylamine (20 mL) was bubbled with $N_2$ for 10 min and then the resulting solution was heated at 110 °C overnight in an inert atmosphere. The volatile was evaporated by rotavapor and the residue was subjected to column chromatography on silica gel, eluting with a mixture of $CH_2Cl_2$ and hexane (1/9) to afford a yellow solid (1.04 g, 95%). $^1$H NMR (300 MHz, $CDCl_3$) $\delta$ 8.50–8.47 (dd, $J$ = 8.7 Hz, $J$ = 0.9 Hz, 2H), 8.35 (s, 1H), 7.92 (d, $J$ = 8.4 Hz, 2H), 7.54–7.48 (ddd, $J$ = 8.4 Hz, $J$ = 6.6 Hz, $J$ = 1.3 Hz, 2H), 7.45–7.40 (ddd, $J$ = 8.1 Hz, $J$ = 6.6 Hz, $J$ = 1.1 Hz, 2H), 0.35 (s, 9H).

**9-Ethynylanthracene[12].** To a solution of 9-((trimethylsilyl)-ethynyl)anthracene (960 mg, 3.5 mmol) in THF (30 mL), was added tetrabutylammonium fluoride trihydrate (1.66 g, 5.25 mmol). The mixture was stirred at r.t. for 30 min, then poured into water (50 mL) and extracted with $CH_2Cl_2$ (3 × 50 mL). The solvent was removed under high vacuum to give a pale yellow solid (728 mg, 97%).$^1$H NMR (300 MHz, $CDCl_3$) $\delta$ 8.52–8.49 (dd, $J$ = 8.8 Hz, $J$ = 0.9 Hz, 2H), 8.39 (s, 1H), 7.93 (d, $J$ = 8.4 Hz, 2H), 7.55–7.49 (ddd, $J$ = 8.7 Hz, $J$ = 6.6 Hz, $J$ = 1.3 Hz, 2H), 7.46–7.41 (ddd, $J$ = 8.1 Hz, $J$ = 6.6 Hz, $J$ = 1.3 Hz, 2H), 3.92 (s, 1H).

**Compound 2.** A mixture of **3** (220 mg, 0.27 mmol), 9-ethynylanthracene (161 mg, 0.8 mmol), $Pd(PPh_3)_2Cl_2$ (70 mg, 0.1 mmol), CuI (20 mg, 0.1 mmol) and piperidine (2 mL) in triethylamine (20 mL) was bubbled with $N_2$ for 10 min and then the resulting solution was heated at 110 °C overnight in an inert atmosphere. The volatile was evaporated by rotavapor and the residue was subjected to column chromatography on silica gel, eluting with a mixture of $CH_2Cl_2$ and hexane (1/1) to afford a orange crystalline product (167.6 mg, 64%). $^1$H NMR (300 MHz, $CDCl_3$) $\delta$ 8.90–8.87 (dd, $J$ = 8.6 Hz, $J$ = 0.9 Hz, 4H), 8.40 (s, 2H), 7.95 (d, $J$ = 8.3 Hz, 4H), 7.58–7.52 (ddd, $J$ = 8.7 Hz, $J$ = 6.6 Hz, $J$ = 1.3 Hz, 4H), 7.48–7.43 (ddd, $J$ = 8.3 Hz, $J$ = 6.6 Hz, $J$ = 1.1 Hz, 4H), 3.69 (t, $J$ = 7.5 Hz, 8H), 1.72 (m, 8H), 1.15 (m, 24 H), 0.68 (t, $J$ = 7.1 Hz, 12H). $^{13}$C NMR (75.4 MHz, $CDCl_3$) $\delta$ 163.6, 146.3, 133.1, 131.4, 128.8, 128.4, 127.6, 126.8, 125.9, 123.3, 117.3, 116.7, 97.8, 96.8, 91.2, 63.4, 50.1, 31.6, 28.6, 26.3, 22.6, 14.0. ESI-MS Calc. for $C_{68}H_{70}O_2N_4$ 974.5493, found 974.5500.

## Acknowledgements

This work was supported by the Swiss National Science Foundation (grant Nos. 200020-130266/1 and 200021-124643) and EU (FUNMOLS FP7-212942-1).

## Notes and references

1 (*a*) C. Yi, C. Blum, M. Lehmann, S. Keller, S.-X. Liu, G. Frei, A. Neels, J. Hauser, S. Schürch and S. Decurtins, *J. Org. Chem.*, 2010, **75**, 3350; (*b*) H. Li, P. Jiang, C. Yi, C. Li, S.-X. Liu, S. Tan, B. Zhao, J. Braun, W. Meier, T. Wandlowski and S. Decurtins, *Macromolecules*, 2010, **43**, 8058.

2 (*a*) E. Quezada, G. Delogu, D. Vina, L. Santana, G. Podda, M. J. Matos and C. Picciau, *Helv. Chim. Acta*, 2009, **92**, 1309; (*b*) I. Kim and J. Choi, *Org. Biomol. Chem.*, 2009, **7**, 2788; (*c*) L. de Luca, G. Nieddu, A. Porcheddu and G. Giacomelli, *Curr. Med. Chem.*, 2009, **16**, 1.

3 H. Tsuji, C. Mitsui, L. Ilies, Y. Sato and E. Nakamura, *J. Am. Chem. Soc.*, 2007, **129**, 11902.

4 (*a*) Z. Fei, D.-R. Zhu, X. Yang, L. Meng, Q. Lu, W. H. Ang, R. Scopelliti, C. G. Hartinger and P. J. Dyson, *Chem.–Eur. J.*, 2010, **16**, 6473; (*b*) M. Shao, P. Dongare, L. N. Dawe, D. W. Thompson and Y. Zhao, *Org. Lett.*, 2010, **12**, 3050.

5 (*a*) U. Förster, K. Lommel, D. Sauter, C. Grünewald, J. W. Engels and J. Wachtveitl, *ChemBioChem*, 2010, **11**, 664; (*b*) N. Bouquin, V. L. Malinovskii, X. Guégano, S.-X. Liu, S. Decurtins and R. Häner, *Chem.–Eur. J.*, 2008, **14**, 5732.

6 D. Mansell, N. Rattray, L. L. Etchells, C. H. Schwalbe, A. J. Blake, J. Torres, C. Kremer, E. V. Bichenkova, C. J. Barker and S. Freeman, *Org. Biomol. Chem.*, 2010, **8**, 2850.

7 Y. Zhou, C.-Y. Zhu, X.-S. Gao, X.-Y. You and C. Yao, *Org. Lett.*, 2010, **12**, 2566.

8 Y. Li, H.-W. Li, L.-J. Ma, Y.-Q. Dang and Y. Wu, *Chem. Commun.*, 2010, **46**, 3768.

9 H. Maeda, T. Maeda, K. Mizuno, K. Fujimoto, H. Shimizu and M. Inouye, *Chem.–Eur. J.*, 2006, **12**, 824.

10 (*a*) C. Yi, C. Blum, S.-X. Liu, G. Frei, A. Neels, P. Renaud, S. Leutwyler and S. Decurtins, *J. Org. Chem.*, 2008, **73**, 3596; (*b*) C. Yi, C. Blum, S.-X. Liu, G. Frei, A. Neels, H. Stoeckli-Evans, S. Leutwyler and S. Decurtins, *Tetrahedron*, 2008, **64**, 9437; (*c*) C. Yi, C. Blum, S.-X. Liu, Y-F. Ran, G. Frei, A. Neels, H. Stoeckli-Evans, G. Calzaferri, S. Leutwyler and S. Decurtins, *Cryst. Growth Des.*, 2008, **8**, 3004.

11 E. Rivera, M. Belletête, X. X. Zhu, G. Durocher and R. Giasson, *Polymer*, 2002, **43**, 5059.

12 (*a*) Z. Zhao, S. Yu, L. Xu, H. Wang and P. Lu, *Tetrahedron*, 2007, **63**, 7809; (*b*) A. Nierth, A. Y. Kobitski, G. U. Nienhaus and A. Jäschke, *J. Am. Chem. Soc.*, 2010, **132**, 2646.

13 R. Shukla, S. H. Wadumethrige, S. V. Lindeman and R. Rathore, *Org. Lett.*, 2008, **10**, 3587.

14 (*a*) R. Ahlrich, M. Bär, M. Häser, H. Horn and C. Kölmel, *Chem. Phys. Lett.*, 1989, **162**, 165; (*b*) R. Bauernschmitt and R. Ahlrich, *Chem. Phys. Lett.*, 1996, **256**, 454; (*c*) R. Bauernschmitt, M. Häser, O. Treutler and R. Ahlrich, *Chem. Phys. Lett.*, 1997, **264**, 573.

15 C. W. Marquardt, S. Grunder, A. Błaszczyk, S. Dehm, F. Hennrich, H. v. Löhneysen, M. Mayor and R. Krupke, *Nat. Nanotechnol.*, 2010, **5**, 863.

16 S. Hamai and F. Hirayama, *J. Phys. Chem.*, 1983, **87**, 83.

17 D. Magde, R. Wong and P. G. Seybold, *Photochem. Photobiol.*, 2002, **75**, 327.

18 G. Meszaro, C. Li, I. Pobelov and Th. Wandlowski, *Nanotechnology*, 2007, **18**, 424004.

19 *Stoe & Cie. X-Area V1.35 & X-RED32 V1.31 Software*, Stoe & Cie GmbH, Darmstadt, Germany, 2006.

20 G. M. Sheldrick, *Acta Crystallogr., Sect. A: Found. Crystallogr.*, 2008, **A64**, 112.

 